Available online at www.sciencedirect.com

SCIENCE DIRECT

Biochimica et Biophysica Acta 1706 (2005) 232–238

BIOCHIMICA ET BIOPHYSICA ACTA BBA

http://www.elsevier.com/locate/bba

pH dependence of charge transfer between tryptophan and tyrosine in dipeptides

Steven Y. Reece, JoAnne Stubbe*, Daniel G. Nocera*

Department of Chemistry, 6-335, 77 Massachusetts Avenue, Massachusetts Institute of Technology, Cambridge, Massachusetts 02139-4307, USA

Received 18 August 2004; received in revised form 11 November 2004; accepted 15 November 2004
Available online 18 December 2004

Abstract

Time-resolved absorption spectroscopy has been employed to study the directionality and rate of charge transfer in W–Y and Ac-W–Y dipeptides as a function of pH. Excitation with 266-nm nanosecond laser pulses produces both W· (or $[\cdot WH]^+$, depending on pH) and Y·. Between pH 6 and 10, W· to was found to oxidize Y with $k_{X\cdot}=9.0\times10^4$ s^{-1} and 1.8×10^4 s^{-1} for the W–Y and Ac-W–Y dipeptide systems, respectively. The intramolecular charge transfer rate increases as the pH is lowered over the range 6>pH>2. For 10<pH<12, the rate of radical transport for the W–Y dipeptide decreases and becomes convoluted with other radical decay processes, the timescales of which have been identified in studies of control dipeptides Ac-F–Y and W–F. Further increases in pH prompt the reverse reaction to occur, $W–Y\cdot \rightarrow W\cdot–Y^-$ (Y^-, tyrosinate anion), with a rate constant of $k_{X\cdot}=1.2\times10^5$ s^{-1}. The dependence of charge transfer directionality between W and Y on pH is important to the enzymatic function of several model and natural biological systems as discussed here for ribonucleotide reductase.

Keywords: Tyrosine; Tryptophan; Radical; Proton-coupled electron transfer; Ribonucleotide reductase

1. Introduction

Radical initiated electron transfer between tryptophan and tyrosine residues in proteins has been extensively studied [1,2], with particular focus on lysozyme enzymes [3–5]. The observation of these two amino acids interacting with each other as part of a natural enzymatic electron transfer (ET) pathway, however, has been limited to only a few systems. *A. nidulans* photolyases possess a W triad (W390, W367, and W314) through which a flavin generated hole passes to generate a tyrosine radical located at the surface of the protein [6]. In the absence of exogenous reductants, Y· is generated in <500 ns, and reverse ET regenerates Y, suggesting regulated radical transport between Y and W [7,8]. Y· hole transfer in the reverse direction is slowed in D_2O, thereby implicating the role of a proton in mediating the ET, though the basis for the increase in Y· lifetime has yet to be determined. Electron transfer between cytochrome *c* and cytochrome *c* peroxidase modified with a K^+ binding site (CcPK2) is also believed to be modulated by an equilibrium between tryptophan cation and tyrosyl radicals [9]. Population of the K^+ binding site shifts the equilibrium from $[\cdot WH]^+$ towards the Y·, which in turn retards the rate of cytochrome *c* oxidation by the compound I intermediate of cytochrome *c* peroxidase.

We have been interested in the redox interplay between Y and W in class I ribonucleotide reductases (RNRs). Class I RNRs are thought to be composed of a 1:1 complex of two homodimeric subunits, R1 and R2. A stable ·Y122 located on R2 is transported to a cysteine (C439) contained in R1. The Y122 and C439 residues are proposed to be separated by 35 Å, based on a docking model generated from the individual crystal structures of R1 and R2 using shape complementarities and electrostatics [10]. The radical initiation at C439 is thought to occur reversibly between

* Corresponding authors. Tel.: +1 617 253 5537; fax: +1 617 253 7670.
E-mail addresses: nocera@mit.edu (D.G. Nocera), stubbe@mit.edu (J. Stubbe).

0005-2728/$ - see front matter © 2004 Elsevier B.V. All rights reserved.
doi:10.1016/j.bbabio.2004.11.011

the two subunits on every enzymatic turnover [11]. The amino acids along the pathway (tyrosine, tryptophan, and cysteine) require changes in protonation state to become transiently oxidized [12] and control the directionality of radical propagation, implicating proton-coupled electron transfer (PCET) for some of the radical propagation steps [13,14]. Importantly, tryptophan W48 is positioned between Y122, the initial site of radical generation, and Y356, the conduit for radical transport between R1 and R2 [15]. Mutagenesis studies suggest that W48 is needed for the forward propagation of the radical into the active site [16]. This implicates ·Y122 oxidation of W48 to produce a radical, which in turn is proposed to oxidize Y356. Moreover, studies of the assembly of the diiron cofactor of R2 provide direct spectroscopic evidence for $[\cdot W48H]^+$ radical [17–20] and suggest it to be directly involved in Y122 oxidation [18]. Together, these studies suggest that W–Y electron transfer is needed for radical propagation in RNR and that the protonation state of W48 may be important in controlling the direction of radical propagation.

To gain insight into W–Y radical transport, we have undertaken detailed time-resolved laser spectroscopy studies of the pH dependence of the rates of radical transfer between tryptophan and tyrosine in W–Y and Ac-W–Y dipeptides. The kinetics of W·–Y→W–Y· has been examined in dipeptides using either flash photolysis or pulsed radiolysis as the radical generator. At or near pH 7, the reaction rate is observed to occur with a rate constant of $9\pm5\times10^4$ s^{-1} [21–27]. Studies of the intermolecular reaction of L-tryptophan and L-tyrosine in solution show that tyrosine radicals can oxidize tryptophan at pH 1.1 and possibly at 12.5, but between these values, tryptophan radicals oxidize tyrosine [28]. The pH dependence for radical transport through proline has been found to be constant between pH 6.5 and 11 and increase linearly below pH 6 [29]. We now show that the directionality of radical transport in W–Y is controlled by pH and suggest the importance of the W protonation state on the directionality of PCET in RNRs.

2. Materials and methods

L-Tryptophanyl-tyrosine (W–Y), L-tryptophanyl-phenylalanine (W–F) (Sigma), *N*-α-acetyl-L-tryptophan (Ac-Trp-OH), *N*-α-acetyl-L-phenylalanine (Ac-F-OH), L-tyrosine *tert*-butyl ester (H-Tyr-O-t-Bu), 1-hydroxybenzotriazole (HOBt) (NovaBiochem), 1-(3-dimethylamino-propyl)-3-ethylcarbodiimide hydrochloride (WSC·HCl), and *N*-methylmorpholine (NMM) (Aldrich) and trifluoroacetic acid (TFA, 99.9%) (J. T. Baker) were used as received.

2.1. *N*-α-Acetyl-L-tryptophanyl-L-tyrosine (Ac-W–Y)

Ac-Trp-OH (301 mg, 1.22 mmol, 1.0 eq), H-Tyr-O-t-Bu (290 mg, 1.22 mmol, 1.0 eq), WSC·HCl (258 mg, 1.34 mmol, 1.1 eq), HOBt (182 mg, 1.34 mmol, 1.1 eq), and NMM (550 μL, 4.88 mmol, 4.0 eq) were combined in a round bottom flask with 100 mL of chloroform and stirred overnight. The reaction solution was extracted in a separatory funnel with 2×50 mL 10% citric acid, 1.0 M sodium bicarbonate, and water. The organic layer was dried over magnesium sulfate and the solvent removed in vacuo to yield a clear oil. The oil was dissolved in a minimal amount of ethyl acetate, loaded onto a chromatotron plate (silica gel, 2 mm), and eluted with ethyl acetate. Three bands were observed under a UV lamp (254 nm). The first band to elute was collected and the solvent removed in vacuo to yield a clear oil. The oil was dissolved in 1% MeOH/10%TFA/CH_2Cl_2 (100 mL) and stirred for 1 h during which time the solution turned pink. The solvent was removed in vacuo, resulting in a tan oil that was placed under high vacuum overnight. It was then dissolved in a minimal amount of ethyl acetate and loaded onto another chromatotron plate (silica gel, 2 mm). The plate was allowed to dry to remove the ethyl acetate and was then eluted with 5–6% MeOH/CH_2Cl_2 (1% acetic acid). The most intense band was collected and the solvent removed under high vacuum. The tan oil was dissolved in 150 mL ethyl acetate, washed with 2×75 mL water to remove any remaining acetic acid, dried over $MgSO_4$, and the solvent removed in vacuo to yield a tan oil that solidified over a few days (205 mg, 0.500 mmol, 41%). ^{1}H NMR (300 MHz, CD_3OD, 25 °C) δ=7.93 (d, 1H, N-H), 7.57 (d, 1H, indole-H), 7.30 (d, 1H, ind-H), 7.15–6.61 (m, 7H, ind-H and phenol-H), 4.67 (m, 1H, W-CH), 4.56 (m, 1H, Y-CH), 3.28–2.80 (m, 4H, W-CH_2 and Y-CH_2), 1.86 (s, 3H, Ac-CH_3); anal. calcd for $C_{22}H_{23}N_3O_5$: C, 64.54; H, 5.66; N, 10.26; found: C, 64.47; H, 5.71; N, 10.15.

2.2. *N*-α-Acetyl-L-phenylalanyl-L-tyrosine (Ac-F–Y)

Ac-Phe-OH (291 mg, 1.40 mmol, 1.0 eq), H-Tyr-O-t-Bu (333 mg, 1.40 mmol, 1.0 eq), WSC·HCl (296 mg, 1.54 mmol, 1.1 eq), HOBt (208 mg, 1.54 mmol, 1.0 eq), and NMM (631 μL, 5.60 mmol, 4.0 eq) were dissolved in chloroform (125 mL) and stirred overnight in a round bottom flask. The reaction solution was extracted in a separatory funnel with 2×50 mL 10% citric acid, 1.0 M sodium bicarbonate, and water. The organic layer was dried over magnesium sulfate and the solvent removed under rotary evaporation to yield a clear oil that eluted as one spot by TLC (Si gel, ethyl acetate). The oil was dissolved in 1% MeOH/10% TFA/CH_2Cl_2 (100 mL) and stirred for 1 h. The solvents were removed in vacuo, and the remaining residue was placed under high vacuum overnight to yield a clear oil which crystallized from ethyl acetate as a white solid (450 mg, 1.26 mmol, 90%). ^{1}H NMR (300 MHz, CD_3OD, 25 °C) δ=8.08 (d, 1H, N-H), 7.21 (m, 5H, F-C_6H_5), 7.02 (m, 2H, Phenol-H), 6.67 (m, 2H, Phenol-H), 4.58 (m, 2H, F-CH and Y-CH), 3.16–2.71 (m, 4H, F-CH_2, and F-CH_2), 1.84 (s, 3H, Ac-CH_3); anal. calcd for $C_{19}H_{20}N_2O_5$: C, 64.04; H, 5.66; N, 7.86; found: C, 64.15; H, 5.61; N, 7.76.

2.3. Physical measurements

^{1}H NMR spectra were recorded on a Varian 300 MHz NMR at the MIT Department of Chemistry Instrumentation Facility (DCIF). UV–vis absorption spectra were recorded on a Cary 17D spectrophotometer.

Pump light for transient absorption (TA) measurements was provided by an Infinity Nd:YAG laser (Coherent) running at 20 Hz. The set-up of the instrument was slightly modified from that previously described [30]. The second harmonic was frequency doubled with an XPO-UV frequency doubling crystal (Coherent) to produce a 266-nm laser pulse with a beam diameter of 4 mm, 2.5 ns pulse width, and pulse energy of ~500 μJ. A 75-W Xe arc lamp (unpulsed, PTI) provided the probe light. The signal light passed through a Triax 320 spectrometer, where it was dispersed by a 300×500 blazed grating and collected with either an intensified gated CCD camera (ICCD, CCD 30-11, Andor Technology, 1024×256 pixels, 26 μm^2) for TA spectra or a photomultiplier tube (PMT) for TA kinetics at a single wavelength. PMT outputs were collected and averaged with a 1 GHz oscilloscope (LeCroy 9384CM). To produce a TA spectrum, a series of four spectra were taken: I_F (pump on/probe off), I (pump on/probe on), I_B (pump off/probe off), and I_0 (pump off/probe on). Uniblitz shutters driven by delay generators (DG535, Stanford Research Systems) and T132 Uniblitz shutter drivers were used to block the pump and probe light in this sequence using a TTL trigger from the Q-switch of the laser. Transient spectra were corrected for fluorescence and background light using these spectra by the calculation: $\Delta OD = \log[(I_0-I_B)/(I-I_F)]$. The spectra reported are the average of 2500 of the four-spectra sequences. The instrument control and data analysis were performed by software written in LabView. For photochemical measurements, a sample ground state absorbance of 1 at 266 nm (~0.3 mM) was used in order to maximize signal and minimize first and second order radical reactions. Aqueous samples were prepared in deionized water with 10 mM phosphate, pH adjusted with 1 M NaOH or 1 M HCl, and flowed through a 1-cm cell with continual oxygen bubbling.

3. Results and discussion

The transient absorption spectrum of laser excited (λ_{exc}=266 nm) solutions of W–Y at pH 7.8 is dominated by the dynamics of the decay of the ^{3}W* excited state (λ_{max}=450 nm [31]) at short times (10 ns–1 μs). After 2 μs, all triplet states have decayed to the ground state or reacted with dissolved O_2 to reveal the transient absorption spectrum shown in Fig. 1. Two prominent transient signals are observed with λ_{max}=410 and 510 nm; these maxima coincide with the maxima for Y· and W· radicals, respectively (ε_{410}(Y·)=2750±200 [32]; ε_{510}(W·)=1800±50 [33]). The time evolution of the absorption

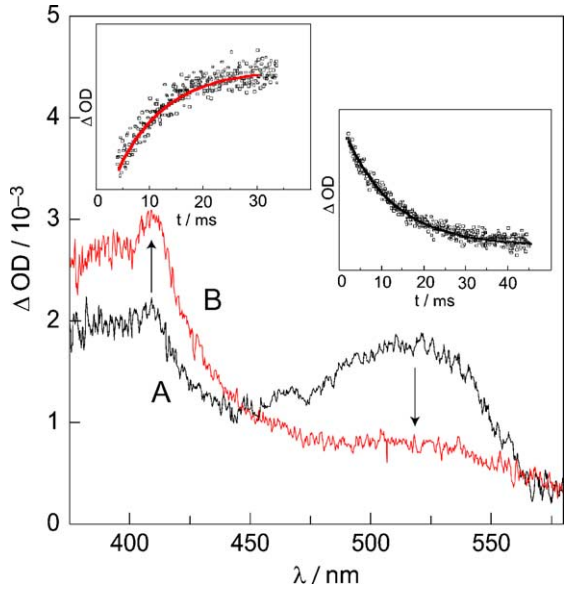

Fig. 1. Transient absorption spectrum following 266-nm laser excitation (fwhm=3 ns) of W–Y solution at pH 7.8 at 2 (——; trace A) and 20 (——; trace B) μs. Insets: Single wavelength kinetics traces (detection wavelength indicated by arrows) for the appearance of the 410 nm (Y·) signal and the disappearance of the 510 nm (W·) signal.

spectrum is revealed with single wavelength kinetics measurements. As shown in the inset, the W· radical decays with a rate constant of 8.6×10^4 s^{-1} and Y· appears on a commensurate time scale ($k_{X\cdot}$=1.1×10^5 s^{-1}). Other intra- and intermolecular radical decay process of Y and W were examined by measuring the kinetics of control peptides Ac-F–Y and W–F, respectively. We find that the decay processes of photogenerated radicals in the control dipeptides are slow and do not contribute significantly to the transient signals shown in Fig. 1. The rate constants for radical transport agree well with the rates previously observed for W·–Y→W–Y· transfer at neutral pH [21–27].

A similar result is obtained for Ac-W·–Y→Ac-W–Y·, with a slightly attenuated rate for radical transfer ($k_{X\cdot}$=1.8×10^4 s^{-1}). Because radical transport is slower in the acylated peptide, other radical decay processes become competitive for Y· decay but not for W· decay, as determined from the control peptides. For this reason, the kinetics of the Ac-W·–Y→Ac-W–Y· reaction (over all pH ranges) was determined from monitoring the 510-nm transient signal corresponding to W·. In the case of the native W–Y dipeptide, the N-terminus is protonated, and thus, electron transport occurs across a favorable dipole. Ab initio calculations show that the removal of the positive charge at the N-terminus of dipeptides significantly reduces the dipole moment [34]; we therefore expect the electron transfer rate to be reduced, as observed, in the Ac-W–Y peptide. These observations are consistent with electron transfer in model peptides, which have been shown to exhibit enhanced rates for charge transfer when the direction of electron movement coincides favorably with the peptide dipole [35,36].

The overall profile of the transient absorption spectrum and the kinetics for radical transport are maintained over a pH range of 6 to 10. Below pH 6, the transient signal for tryptophan radical red-shifts from 510 nm to 560 nm, as shown in Fig. 2. At pH 3.1, the transient absorption spectrum is dominated by the 560-nm feature, which is consistent with the production of a protonated tryptophan radical, $[\cdot WH]^+$ (ε_{560}=3000±150, pK_a=4.3 [37]). At intermediate pH, a signal is observed with a maximum that lies between the 510 and 560 nm signals for W· and $[\cdot WH]^+$, respectively. The transient signal at pH=4.3=pK_a ($[\cdot WH]^+$) is shown in Fig. 2 and is the superposition of nearly 1:1 contributions of the $[\cdot WH]^+$ and W· transient signals.

The rate for radical transport from W to Y in both W–Y and Ac-W–Y steadily increases as the pH is lowered from 6 to 2. However, below pH ~4, the radical transport in W–Y becomes fast enough to be convoluted and masked by the decay of ^{3}W*. Owing to the slower radical transport in Ac-W–Y (vide supra), rate constants could be measured to pH ~2. At pH 2.35, Ac-$[\cdot WH]^+$–Y→Ac-W–Y· proceeds with a rate constant of 1.5×10^5 s^{-1}, as measured by the disappearance of the 560 nm component. For the control peptide, the W·/$[\cdot WH]^+$ decay is invariant with pH and slow with respect to this time scale. Thus, specious radical decays do not interfere with these measurements. The observed steady increase in the rate of radical transport from W to Y with decreasing pH is consistent with similar previous studies in the Trp-Pro-Tyr peptide probed by pulse radiolysis [29].

At the other end of the pH scale, the radical transport rate constant decreases over the range 10<pH<11.6 for W–Y and 10<pH<12.2 for Ac-W–Y. The rate for radical transport becomes sufficiently slow that other first and second order radical decay processes, as measured for the control peptides, prevent the extraction of an electron rate constant from the decay trace of the 510-nm transient. A further increase in pH beyond 12 is accompanied by opposite behavior in the time evolution of the transient absorption spectrum of W–Y. Namely, the 510-nm transient signal of W· appears with the concomitant disappearance of the 410 nm signal of Y·, indicating the reverse reaction, W–Y·→ W·–Y$^-$, where Y$^-$ represents the deprotonated tyrosinate anion. The rate constant for this reverse reaction is $k_X^{rev}=1.2\times10^5$ s^{-1}.

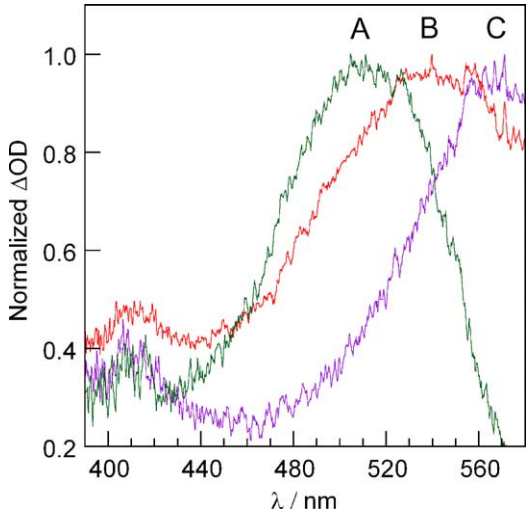

Fig. 2. Transient absorption spectrum 2 μs after 266-nm laser excitation (fwhm=3 ns) of Ac-W–Y solution at pH 7.2 (——; A), 4.3 (——; B), and 3.1 (——; C).

Fig. 3 summarizes the pH dependence of the rates of the radical transport reactions of W–Y and Ac-W–Y. For both peptides, radical transport from W to Y is preferred for pH 6–10, and the rate constant for the reaction is invariant over this pH range. At the endpoints of the pH plateau, the rate constant monotonically increases as the pH is lowered below 6 and decreases as the pH is raised above 10. For pH >12, the reaction reverses and radical transport from Y to W is favored. This reversal of radical transport in W–Y dipeptides has escaped detection by laser photolysis and only been observed previously by pulse radiolysis at pH 13 [28].

Insight into the rates and direction of radical transport between W and Y dipeptides is provided by analysis of the W·/W and Y·/Y reduction potentials. The solid line in Fig. 3 is the difference in these reduction potentials, $\Delta E=E_p(W\cdot/W)-E_p(Y\cdot/Y)$, as calculated from the differential pulse voltammetry measurements of Tommos et al. which are also summarized in Fig. 3 [38]. For pH>6, the rate constants are approximated well by the driving force dependence of the radical transport. We ascribe the invariance of the rate constant for pH 6–10 to the constant value of ΔE over this pH range. For pH>10, the hydroxyl group of Y is deprotonated and $E_p(Y\cdot/Y)$ becomes constant with pH, whereas $E_p(W\cdot/W)$ continues to decrease monotonically (see Fig. 4). The confluence of these two trends causes the driving force for radical transfer between W· and Y to decrease in this pH range. The rate constant for radical transfer is expected to reflect this decrease until $E_p(Y\cdot/Y)=E_p(W\cdot/W)$ at pH 10.9; this is observed in Fig. 3. For pH>10.9, the direction of radical transport reverses as oxidation of W by Y· is preferred.

A perplexing increase in rate is observed for pH 2–6. Over this pH range, protonation of W· to produce $[\cdot WH]^+$ is favorable, and the reduction potential accordingly becomes pH independent (see Fig. 4). The increased oxidizing power of the $[\cdot WH]^+$ radical, however, is offset by the increased difficulty in oxidizing Y, leading to a mild reduction in the driving force over this pH range. On this basis, the rate for Y oxidation by W·/$[\cdot WH]^+$ should slowly decrease, but this expectation is not met. The rate of Y oxidation increases with decreasing pH to pH 2. We ascribe the rate enhancement in part to the further augmentation of the peptide dipole upon protonation of the tryptophan residue. The convergence of the

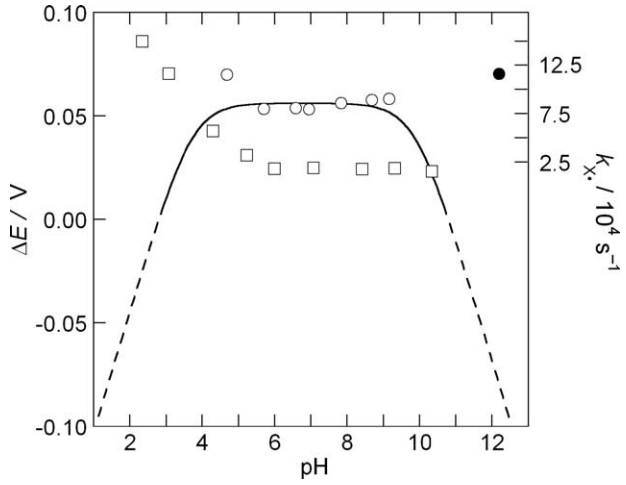

Fig. 3. Rates of radical transport vs. pH for dipeptides W•/[•WH]$^+$–Y→W–Y• (○); Ac-W•/[Ac-•WH]$^+$–Y→Ac-W–Y• (□); and W–Y•→W•–Y$^-$ (●). The solid line is the $\Delta E = E_p(W•/W) - E_p(Y•/Y)$, calculated from the differential pulse voltammetry measurements shown.

Y•/Y and [•WH]$^+$/W reduction potentials at pH 2.8 causes the driving force for radical transport to decrease to the point that the reaction becomes thermoneutral. A further decrease in the pH should shift the energetics to favor the W–Y•→W•–Y reaction. Indeed, radical transport from Y to W in at very acidic pH (=1) has been observed for the intermolecular reaction between W and Y in pulse radiolysis experiments [28].

4. Conclusions

The results reported herein have mechanistic implications to radical-induced cofactor assembly and nucleotide reduction processes of RNR. Fig. 5 shows the diiron cofactor and selected amino acid residues that comprise the beginning of the 35 Å radical transport pathway that spans the R2 and R1 subunits of class I RNRs. The figure highlights the location of W48 between Y122 and Y356 and the proximity of W48 to D237. The potential importance of W48 and [•W48H]$^+$ was first noted by Nordlund and Eklund [39,40], who proposed that the Fe1→H118→D237→W48 pathway in R2 could be mechanistically important in cofactor assembly and nucleotide reduction, based on the structurally analogous and spectroscopically well-characterized Fe(heme)→H→D→W ET pathway in cytochrome *c* peroxidase. Subsequent studies have suggested that the PCET pathway in the assembly process is shared with part of the ET pathway in the nucleotide reduction process [13]. The failure of previous kinetic studies to the disappearance and reappearance of Y• during turnover have led to the proposal that PCET occurs in the forward and reverse direction along the 35 Å pathway every time nucleotide reduction occurs. The studies reported herein show that the protonation state of W48 can control the rate and direction of radical transport by modulating the Y122→W48→Y356 interactions. D237 provides a site to establish PCET by coupling electron transfer along the radical transport pathway to proton transfer to or from W48. As has been recently noted [41], a conserved residue, R236, may also influence local pK_a by interacting directly with D237 or other redox active residues along the pathway.

By implicating D237 in radical transport, a PCET pathway is constructed whereby proton transfer is orthogonal to the electron transfer pathway. The modulation of electron transport by a proton along an orthogonal path appears to be an emerging trend in the PCET events of biology. A crucial tyrosine, Y_Z (Y161), in Photosystem II

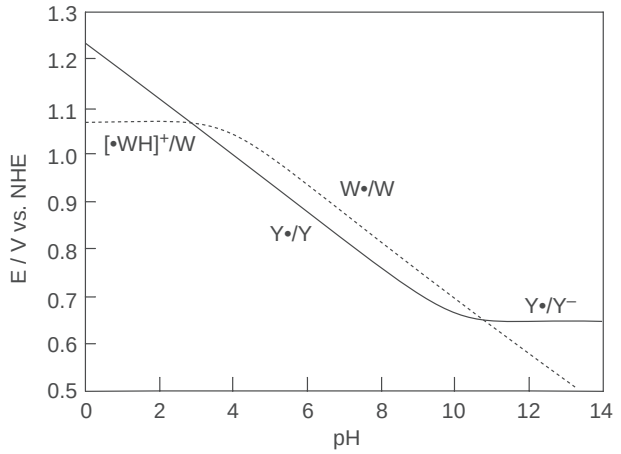

Fig. 4. $E_p(W•/W)$ and $E_p(Y•/Y)$ reduction potentials vs. pH as measured by differential pulse voltammetry (Ref. [38]) of aqueous solutions of Ac-W–NH_2 and Ac-Y–NH_2.

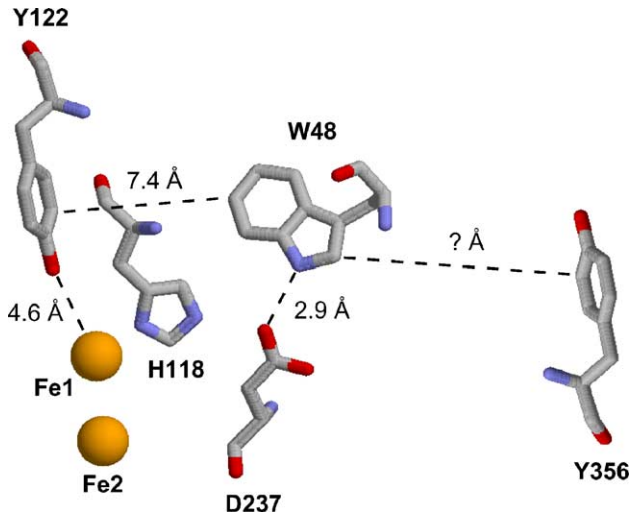

Fig. 5. The Y122↔W48↔Y356 pathway of R2 proposed to be important for the assembly of the diiron cofactor and radical transport leading to nucleotide reduction. The radical transfer pathway and distances are from the crystal structure of oxidized R2 at 1.4-Å resolution [50]. The last 35 amino acids of the C-terminal tail of R2, in which Y356 resides, are thermally labile and undetectable in available crystal structures.

(PSII) is the linchpin that manages electron and proton flow in the conversion of the primary light absorption event at the P680 chlorophylls into the multielectron activation of water at the oxygen-evolving complex (OEC) [42,43]. Histidine H190 positioned off of the ET pathway provides a basic residue that is essential for effective oxidation of Y_Z by $P680^+$. The neutral radical, $\cdot Y_Z$, is the primary oxidant that steps the tetranuclear manganese cluster, one electron/one proton at a time, through each of the four S states of the Kok cycle [44,45]. The stoichiometry of electron and proton release, however, has yet to be resolved definitively [45,46]. In RNR, PCET involves tyrosyl radicals produced from orthogonal proton and electron pathways; but unlike PSII, the tyrosyl radical participation is not direct. Instead, W48 sandwiched between tyrosines provides the necessary coupling between the proton and electron. By enforcing the appropriate pK_a on W48, the protein can control the direction of radical transport among tyrosines, which are proposed to be involved in radical initiation of nucleotide reduction and di-iron tyrosyl radical assembly. We are currently developing new donor–acceptor architectures [47] and biophysical methods [48,49] that will allow us to directly examine PCET arising from coupling between orthogonal proton and electron pathways in model and natural systems.

Acknowledgments

We thank Michelle C. Y. Chang and Niels H. Damrauer for helpful discussions. We thank the National Institutes of Health for support of this work GM47274 (DGN) and GM29595 (JS).

References

[1] J. Butler, E.J. Land, W.A. Pruetz, J.A. Swallow, Charge transfer between tryptophan and tyrosine in proteins, Biochim. Biophys. Acta 705 (1982) 150–162.
[2] R. Joshi, T. Mukherjee, Effect of solvent viscosity, polarity and pH on the charge transfer between tryptophan radical and tyrosine in bovine serum albumin: a pulse radiolysis study, Biophys. Chemist. 103 (2003) 89–98.
[3] M. Weinstein, Z.B. Alfassi, M.R. DeFelippis, M.H. Klapper, M. Faraggi, Long range electron transfer between tyrosine and tryptophan in hen egg-white lysozyme, Biochim. Biophys. Acta 107 (1991) 173–178.
[4] K. Bobrowski, J. Holcman, J. Poznanski, K.L. Wierzchowski, Pulse radiolysis studies of intramolecular electron transfer in model peptides and proteins: 7. Trp$\cdot \rightarrow$TyrO$\cdot$ radical transformation in hen egg-white lysozyme. Effects of pH, temperature, Trp62 oxidation and inhibitor binding, Biophys. Chemist. 63 (1997) 153–166.
[5] M. Stuart-Audette, Y. Blouquit, M. Faraggi, C. Sicard-Roselli, C. Houée-Leven, P. Jollés, Re-evaluation of intramolecular long-range electron transfer between tyrosine and tryptophan in lysozymes. Evidence for the participation of other residues, Eur. J. Biochem. 270 (2003) 3565–3571.
[6] A. Sancar, Structure and function of DNA photolyase and cryptochrome blue-light photoreceptors, Chem. Rev. 103 (2003) 2203–2238.
[7] C. Aubert, P. Mathis, A.P.M. Eker, K. Brettel, Intraprotein electron transfer between tyrosine and tryptophan in DNA photolyase from *Anacystis nidulans*, Proc. Natl. Acad. Sci. U. S. A. 96 (1999) 5423–5427.
[8] C. Aubert, K. Brettel, P. Mathis, A.P.M. Eker, A. Boussac, EPR detection of the transient tyrosyl radical in DNA photolyase from *Anacystis nidulan*, J. Am. Chem. Soc. 121 (1999) 8659–8660.
[9] T.P. Barrows, B. Bhaskar, T.L. Poulos, Electrostatic control of the tryptophan radical in cytochrome *c* peroxidase, Biochemistry 43 (2004) 8826–8834.
[10] U. Uhlin, H. Eklund, Structure of ribonucleotide reductase protein R1, Nature 370 (1994) 533–539.
[11] J. Ge, G. Yu, M.A. Ator, J. Stubbe, Pre-steady-state and steady-state kinetic analysis of *E. coli* class I ribonucleotide reductase, Biochemistry 42 (2003) 10071–10083.
[12] J. Stubbe, W.A. van der Donk, Protein radicals in enzyme catalysis, Chem. Rev. 98 (1998) 705–762.
[13] J. Stubbe, D.G. Nocera, C.S. Yee, M.C.Y. Chang, Radical initiation in the class I ribonucleotide reductase: long-range proton-coupled electron transfer? Chem. Rev. 103 (2003) 2167–2201.
[14] R.I. Cukier, D.G. Nocera, Proton-coupled electron transfer, Annu. Rev. Phys. Chem. 49 (1998) 337–369.
[15] M.C.Y. Chang, C.S. Yee, J. Stubbe, D.G. Nocera, Turning on ribonucleotide reductase by light-initiated amino acid radical generation, Proc. Natl. Acad. Sci. U. S. A. 101 (2004) 6882–6887.
[16] U. Rova, K. Goodtzova, R. Ingermarson, G. Behravan, A. Gräslund, L. Thelander, Evidence by site-directed mutagenesis supports long-range electron transfer in mouse ribonucleotide reductase, Biochemistry 34 (1995) 4267–4275.
[17] J.M. Bollinger Jr., D.E. Edmonson, B.H. Huynh, J. Filley, J.R. Norton, J. Stubbe, Mechanism of assembly of the tyrosyl radical-dinuclear iron cluster cofactor of ribonucleotide reductase, Science 253 (1991) 292–298.
[18] J.M. Bollinger Jr., W.H. Tong, N. Ravi, B.H. Huynh, D.E. Edmondson, J. Stubbe, Mechanism of assembly of the tyrosyl radical-diiron(III) cofactor of *E. coli* ribonucleotide reductase: 3. Kinetics of the limiting Fe^{2+} reaction by optical, EPR, and Mössbauer spectroscopies, J. Am. Chem. Soc. 116 (1994) 8024–8032.
[19] J. Baldwin, C. Krebs, B.A. Ley, D.E. Edmondson, B.H. Huynh, J.M. Bollinger Jr., Mechanism of rapid electron transfer during oxygen activation in the R2 subunit of *Escherichia coli* ribonucleotide reductase: 1. Evidence for a transient tryptophan radical, J. Am. Chem. Soc. 122 (2000) 12195–12206.
[20] C. Krebs, S. Chen, J. Baldwin, B.A. Ley, U. Patel, D.E. Edmondson, B.H. Huynh, J.M. Bollinger Jr., Mechanism of rapid electron transfer during oxygen activation in the R2 subunit of *Escherichia coli* ribonucleotide reductase: 2. Evidence for and consequences of blocked electron transfer in the W48F variant, J. Am. Chem. Soc. 122 (2000) 12207–12219.
[21] O.B. Morozova, A.V. Yurkovskaya, H.-M. Vieth, R.Z. Sagdeev, Intramolecular electron transfer in tryptophan–tyrosine peptide in photoinduced reaction in aqueous solution, J. Phys. Chem., B 107 (2003) 1088–1096.
[22] O.B. Morozova, A.V. Yurkovskaya, Y.P. Tsentalovich, M.D.E. Forbes, R.Z. Sagdeev, Time-resolved CIDNP study of intramolecular charge transfer in the dipeptide tryptophantyrosine, J. Phys. Chem., B 106 (2002) 1455–1460.
[23] Q.-H. Song, Q.-X. Gou, S.-D. Yao, N.-Y. Lin, Comparison of intermediates of tryptophan, tyrosine, and their dipeptide induced by UV light and $SO_4\cdot^-$, Res. Chem. Intermed. 28 (2002) 329–335.
[24] M. Faraggi, M.R. DeFelippis, M.H. Klapper, Long-range electron transfer between tyrosine and tryptophan in peptides, J. Am. Chem. Soc. 111 (1989) 5141–5145.

[25] W.A. Prütz, E.J. Land, R.W. Sloper, Charge transfer in peptides, J. Chem. Soc., Faraday Trans. 1 77 (1981) 281–292.
[26] W.A. Prütz, F. Siebert, J. Butler, E.J. Land, A. Menez, T. Montenay-Garestier, Charge transfer in peptides. intramolecular radical transformations involving methionine, tryptophan, and tyrosine, Biochim. Biophys. Acta 705 (1982) 139–149.
[27] R.W. Sloper, E.J. Land, Photoinitiation of one electron reactions in dipeptides and proteins containing tryptophan and tyrosine, Photochem. Photobiol. 32 (1980) 687–689.
[28] J. Butler, E.J. Land, W.A. Prütz, A.J. Swallow, Reversibility of charge transfer between tryptophan and tyrosine, J. Chem. Soc. Chem. Commun. 4 (1986) 348–349.
[29] M.R. DeFelippis, M. Faraggi, M.H. Klapper, Evidence for through-bond long-range electron transfer in peptides, J. Am. Chem. Soc. 112 (1990) 5640–5642.
[30] Z.-H. Loh, S.E. Miller, C.J. Chang, S.D. Carpenter, D.G. Nocera, Excited-state dynamics of cofacial pacman porphyrins, J. Phys. Chem., A 106 (2002) 11700–11708.
[31] D.V. Bent, E. Hayon, Excited state chemistry of aromatic amino acids and related peptides III Tryptophan, J. Am. Chem. Soc. 97 (1975) 2612–2619.
[32] J. Feitelson, E. Hayon, Electron ejection and electron capture by phenolic compounds, J. Phys. Chem. 77 (1973) 10–15.
[33] J.F. Baugher, L.I. Grossweiner, Photolysis mechanism of aqueous tryptophan, J. Phys. Chem. 81 (1977) 1349–1354.
[34] L.R. Wright, R.F. Borkman, Ab initio SCF studies of the peptides Gly-Gly, Gly-Ala, Ala-Gly, and Gly-Gly-Gly, J. Phys. Chem. 86 (1982) 3956–3962.
[35] T.L. Batchelder, R.J. Fox III, M.S. Meier, M.A. Fox, Intramolecular excited state electronic coupling along an α-helical peptide, J. Org. Chem. 61 (1996) 4206–4209.
[36] E. Galoppini, M.A. Fox, Effect of the electric field generated by the helix dipole on photoinduced intramolecular electron transfer in dichromophoric α-helical peptides, J. Am. Chem. Soc. 118 (1996) 2299–2300.
[37] S. Solar, N. Getoff, P.S. Surdhar, D.A. Armstrong, A. Singh, Oxidation of tryptophan and *N*-methylindole by $N_3^{\bullet}$, $Br_2^{\bullet -}$, and $(SCN)_2^{\bullet -}$ radicals in light- and heavy-water solutions: a pulse radiolysis study, J. Phys. Chem. 95 (1991) 3639–3643.
[38] C. Tommos, J.J. Skalicky, D.L. Pilloud, J. Wand, P.L. Dutton, De novo proteins as models of radical enzymes, Biochemistry 38 (1999) 9495–9507.
[39] P. Nordlund, H. Eklund, Structure and function of the *Escherichia coli* ribonucleotide reductase protein R2, J. Mol. Biol. 232 (1993) 123–164.
[40] P. Nordlund, B.M. Sjöberg, H. Eklund, Three-dimensional structure of the free radical protein of ribonucleotide reductase, Nature 345 (1990) 593–598.
[41] M. Kolberga, K.R. Stranda, P. Graff, K.K. Andersson, Structure, function, and mechanism of ribonucleotide reductases, Biochim. Biophys. Acta 1699 (2004) 1–34.
[42] G.T. Babcock, B.A. Barry, R.J. Debus, C.W. Hoganson, M. Atamian, L. McIntosh, I. Sithole, C.F. Yocum, Water oxidation in Photosystem II: from radical chemistry to multielectron chemistry, Biochemistry 28 (1989) 9557–9565.
[43] C. Tommos, G.T. Babcock, Proton and hydrogen currents in photosynthetic water oxidation, Biochim. Biophys. Acta 1458 (2000) 199–219.
[44] C. Tommos, G.T. Babcock, Oxygen production in nature: a light-driven metalloradical enzyme process, Acc. Chem. Res. 31 (1998) 18–25.
[45] W. Junge, M. Haumann, R. Ahlbrink, A. Mulkidjanian, J. Clausen, Electrostatics and proton transfer in photosynthetic water oxidation, Philos. Trans. R. Soc. Lond., B 357 (2002) 1407–1418.
[46] C. Tommos, Electron, proton and hydrogen-atom transfers in photosynthetic water oxidation, Philos. Trans. R. Soc. Lond., B 357 (2002) 1383–1394.
[47] C.J. Chang, M.C.Y. Chang, N.H. Damrauer, D.G. Nocera, Proton-coupled electron transfer: a unifying mechanism for biological charge transport, amino acid radical initiation and propagation, and bond making/breaking reactions of water and oxygen, Biochim. Biophys. Acta 1655 (2004) 13–28.
[48] C.S. Yee, M.C.Y. Chang, J. Ge, D.G. Nocera, J. Stubbe, 2,3-Difluorotyrosine at position 356 of ribonucleotide reductase R2: a probe of long-range proton-coupled electron transfer, J. Am. Chem. Soc. 125 (2003) 10506–10507.
[49] C.S. Yee, M.R. Seyedsayamdost, M.C.Y. Chang, D.G. Nocera, J. Stubbe, Generation of the R2 subunit of ribonucleotide reductase by intein chemistry: insertion of 3-nitrotyrosine at residue 356 as a probe of the radical initiation process, Biochemistry 42 (2003) 14541–14552.
[50] M. Högbom, M. Galander, M. Andersson, M. Kolberg, W. Hofbauer, G. Lassmann, P. Nordlund, F. Lendzian, Displacement of the tyrosyl radical cofactor in ribonucleotide reductase obtained by single-crystal high-field EPR and 1.4-Å x-ray data, Proc. Natl. Acad. Sci. 100 (2003) 3209–3214.